Geochimica et Cosmochimica Acta, Vol. 69, No. 2, pp. 415–425, 2005

0016-7037/05 $30.00 + .00

doi:10.1016/j.gca.2004.06.031

A low-temperature kinetic study of the exsolution of pentlandite from the monosulfide solid solution using a refined Avrami method

HAIPENG WANG,[1] ALLAN PRING,[2,3,*] YUNG NGOTHAI,[1] and BRIAN O'NEILL[1]

[1]School of Chemical Engineering, University of Adelaide, Adelaide, SA 5005, Australia
[2]Department of Mineralogy, South Australian Museum, Adelaide, SA 5001, Australia
[3]School of Earth & Environmental Science, University of Adelaide, Adelaide, SA 5005, Australia

(*Received December* 1, 2003; *accepted in revised form June* 25, 2004)

Abstract—A refined Avrami method, that assumes that the activation energy is a function of reaction extent y, was used to analyze the kinetics of the exsolution of pentlandite from *mss*/pyrrhotite (bulk composition, $(Fe_{0.77}Ni_{0.19})S$) over the temperature range 473 to 573 K. The experimental results show the reaction rates vary from 1.6×10^{-5} to 5.0×10^{-7} s^{-1} at 473 K and from 9.4×10^{-5} to 4.1×10^{-7} s^{-1} at 573 K. Examination of exsolution textures indicated that the mechanism of exsolution did not change significantly over the temperature range investigated. The activation energy (E_a) decreases from 49.6 to 20.7 kJ mol^{-1} over the course of the reaction. The decrease in E_a with y is related to the change in the dominant factor of pentlandite exsolution, from nucleation dominant at the beginning to metal ion diffusion dominant at the end. The classic Avrami method provides average values of kinetic parameters for the overall solid-state reaction while the refined Avrami method provides more a detailed indication of the variation of kinetic parameters over the course of the reaction. Previously published kinetic data for the exsolution of pentlandite from *mss*/pyrrhotite are reevaluated using the refined Avrami method. *Copyright © 2005 Elsevier Ltd*

1. INTRODUCTION

The kinetic behavior of many mineral reactions has been successfully modelled using the Avrami /Arrhenius model, where the activation energy, E_a, is assumed constant during the course of reaction (Wiersma and Rimstidt, 1984; Putnis, 1992). Preliminary analysis of data for the exsolution of pentlandite and pyrrhotite from the monosulfide solid solution (*mss*) indicated that some modification to this classical treatment was necessary for the reactions in the Fe-Ni-S system (Wang et al., 2003; Etschmann et al., 2004). In this system, activation energies are comparatively small and changes in local crystal chemistry are significant. Vyazovkin (2001) noted that the notion that E_a varies with reaction extent, y, can be widely applied and the assumption of a constant E_a is only valid for a small segment of reaction extent (Δy). The Advanced Isoconversional Method (Vyazovkin, 1997; Vyazovkin, 2001) can be used to evaluate the dependence of E_a on reaction extent, y, using integration techniques.

Empirically it is found that the isothermal kinetics of a wide range of mineral reactions can be described by an equation of the general form

$$y = 1 - \exp\,[-(kt)^n] \tag{1}$$

where k is a rate constant, t is the reaction time, y is the reaction extent and n is a time exponent that depends on the reaction mechanism (Burke, 1965; Christian, 1965; Putnis, 1992).

Solid-state reaction kinetics is based on the activated state theory, where the reaction rate can be written as

$$\frac{dy}{dt} = k \cdot f(y) \tag{2}$$

As k, the rate constant in Eqn. 1 is defined in terms of both y and t, it is not a true rate constant in the same sense as it is in Eqn. 2, where k has the unit of s^{-1}.

It is well known that rate constants are exponentially dependent on the inverse of absolute temperature. The dependence of k on temperature has the general form of the Arrhenius equation:

$$k = A \exp\left(-\frac{E_a}{RT}\right) \tag{3}$$

where A is the preexponential constant. The disadvantage of this method is that the value of k depends on the empiric selection of the function $f(y)$ in Eqn. 2 and therefore E_a depends on the choice of rate equation. A number of different forms of rate equation may fit the data equally well, but result in different values of E_a (Vyazovkin and Wright, 1997). A second disadvantage is that it assumes E_a does not change over the course of an isothermal transformation. However, the activation energy needed to stimulate a reactant to an activated state is dependent on local structural features. The local structural environment of reactant atoms usually changes over the course of a reaction. Thus, it is reasonable to believe E_a is a function of y.

An alternative approach is to use the isoconversional methods of Friedman (1964), Ozawa (1965) and Vyazovkin and Lesnikovich (1990) where E_a is evaluated universally. Ozawa (1965) employed the integral approximation of Doyle (1961) to derive the equation:

$$\log \beta = \text{constant} - 0.4567\, E_a/RT_Y \quad (\text{when } E_a/RT_Y > 20) \tag{4}$$

where β is the heating rate; T_Y, the temperature reached when

* Author to whom correspondence should be addressed, at South Australian Museum, Department of Mineralogy, North Terrace, SA 5001, Australia. (Pring.Allan@saugov.sa.gov.au).

reaction extent is $y = Y$. Given the constancy of E_a, the plot of log β vs. the reciprocal absolute temperature at a given reaction extent, $y = Y$, must give a straight line. This is known as the Ozawa isoconversional method and the slope determines the activation energy. The dependence of activation energy on reaction extent, which is caused by the changing physical and mechanical properties of the reaction medium, was further developed by Vyazovkin (2000a).

In the current study on the exsolution of pentlandite from *mss*/pyrrhotite, the *mss*/pyrrhotite is the reaction media and it becomes progressively metal deficient with increasing reaction extent. Most solid-state reactions are multiple-step reactions. The activation energy dependence on reaction extent reflects the variation in relative contributions of each step to the overall reaction rate (Vyazovkin, 2000b). The main purpose of this study is to find a more appropriate formalization to describe the kinetic behavior of pentlandite exsolution from *mss*/pyrrhotite. This method incorporates the notion of E_a dependence on y (Vyazovkin and Dollimore, 1996; Vyazovkin and Wright, 1997; Vyazovkin, 2003). In this paper a refined Avrami model is derived and fitted to the isothermal data.

Pyrrhotite $(Fe,Ni)_{1-x}S$ and pentlandite $(Fe, Ni)_9S_8$ are important constituents of primary nickel sulfide ore deposits. Pentlandite is invariably associated with pyrrhotite. At high temperatures (above 883 K) $(Fe,Ni)_{1-x}S$ has the NiAs structure and is known as the monosulfide solid solution (*mss*). Above 883 K there is complete solid solution between Fe and Ni end members, but below this temperature *mss* breaks down via exsolution of pentlandite with the residual *mss* undergoing metal-vacancy ordering to form pyrrhotite (Naldrett et al., 1967; Misra and Fleet, 1973a; Francis et al., 1976; Vaughan and Craig, 1978; Durazzo and Taylor, 1982). During exsolution the Ni is concentrated into pentlandite, and in nature the host *mss*/pyrrhotite usually contains less than 1 atomic % Ni. In experimental studies, coexisting pyrrhotites can contain up to 25 atomic % Ni replacing Fe, the extent of this substitution depends both on the bulk composition and temperature (Craig, 1973; Misra and Fleet, 1973a,b; Vaughan and Craig, 1978; Etschmann et al., 2004). Experiments have shown that at 503 K the maximum Ni content of *mss* diminishes to 17 atomic % Ni. This value is still much greater than the range of Ni contents for pyrrhotites that coexist with pentlandite in magmatic sulfide deposits, and indicates that chemical readjustments in these sulfides occur at very low temperatures (Naldrett et al., 1967; Craig, 1973; Misra and Fleet, 1973a; Farrell and Fleet, 2002; Etschmann et al., 2004).

The composition and stoichiometry of the exsolved pentlandite is variable, and in nature, atomic Fe: Ni ratios vary from 1:3 to 3:1 but most natural compositions are close to 1:1 (Riley, 1977). The pure Ni and Fe pentlandite end members are not stable and Ni-rich pentlandites have been reported to show some cation deficiency $(Ni,Fe)_{9-x}S_8$ while Fe-rich pentlandites are said to be cation excess $(Fe,Ni)_{9+x}S_8$ (Rajamani and Prewitt, 1973; Vaughan and Craig, 1974, 1978). The nature of this exsolution process has been studied by a number of workers (Francis et al., 1976; Durazzo and Taylor, 1982; Kelly and Vaughan, 1983; Wang et al., 2003; Etschmann et al., 2004). Durazzo and Taylor (1982) and Kelly and Vaughan (1983) performed systematic studies investigating the exsolution textures produced in synthetic materials. They found that the texture was dependent on the annealing time, the temperature, and S fugacity. Early-formed textures depend on the initial degree of supersaturation and solid-state diffusion; the final textures result from further growth and coarsening of early forms and are particularly sensitive to metal diffusion, which is a function of temperature. Kelly and Vaughan (1983) also reported some preliminary kinetic studies on the pentlandite-pyrrhotite system.

Yund and Hall (1970) studied the kinetics of exsolution of pyrite from pyrrhotite. They measured changes in *mss*/pyrrhotite composition by X-ray diffraction and thus were able to estimate extent of pyrite exsolution. The stoichiometry of pure Fe *mss*/pyrrhotite can readily be determined from the cell parameters and the value of the d_{102} spacing of the NiAs subcell (Arnold, 1962; Toulmin and Barton, 1964; Fleet, 1968; Yund and Hall, 1970). Misra and Fleet (1973b) reported similar results for the effects of Ni/Fe substitution on the d_{102} spacing in *mss*/pyrrhotite, but the changes are an order of magnitude greater than those of the M: S (metal to sulfur) ratio. During the exsolution of pentlandite from *mss*/pyrrhotite, not only does the stoichiometry of *mss*/pyrrhotite change but also the Ni/Fe ratio, so Yund and Hall's (1970) method of measuring the extent of reaction from changes in the mss/pyrrhotite cannot be readily used in this case.

Etschmann et al. (2004) undertook detailed studies on the kinetics of exsolution using powder neutron diffraction phase analysis on anneal/quench samples and in situ cooling experiments. The compositions they investigated were restricted to M: S ratio of 1:1 and the kinetics was found to be very rapid. They concluded that these rapid reactions were driven by very rapid nucleation triggered by formation of S vacancies in the *mss* lattice. Heating *mss* with M: S ratio of 1:1 to 573 K produces S vacancies, which provide metal-enriched sites for the nucleation of pentlandite (Etschmann et al., 2004). Only in anneal/quench experiments at low temperatures, $\leq$ 473 K, was the exsolution process slow enough to allow the data to be fitted to a kinetic model and they used the classic Avrami model (Avrami, 1939; Avrami, 1940, 1941; Christian, 1965; Putnis, 1992). Unfortunately, the low temperature data of Estchmann (2004) were very limited and the uncertainties in the phase portions were relatively large. These errors were amplified during model fitting and resulted in large uncertainties in the calculated activation energy.

In this study, we have used similar methods of powder diffraction phase analysis to investigate a more *S*-rich composition $(Fe_{0.77}Ni_{0.19})S$, where metal to sulfur ratio is 49:51. In these experiments, exsolution is somewhat less rapid.

2. EXPERIMENTAL

2.1. Synthesis

The standard silica-tube techniques (Kullerud, 1971; Vaughan and Craig, 1978) were adopted to synthesize the monosulfide solid solution (*mss*). Accurately weighed stoichiometric amounts of Fe (1 mm diameter wire, 99.9+%, Aldrich), Ni (1 mm diameter wire 99.9+%, Aldrich) and S (granules 99.99+%, Aldrich) were sealed under vacuum in 10 mm diameter silica tubes. Bulk compositions of *mss* were selected to give a Ni: Fe of 20:80 and a metal to sulfur ratio M: S = 49:51. The charges were heated slowly to 573 K, then up to 773 and 1073 K, soaking for 12 h at each stage (Etschmann et al., 2004). The slow heating schedule and soaking process were employed to minimize tube failure due to high sulfur vapour pressure above 723 K. The tubes were

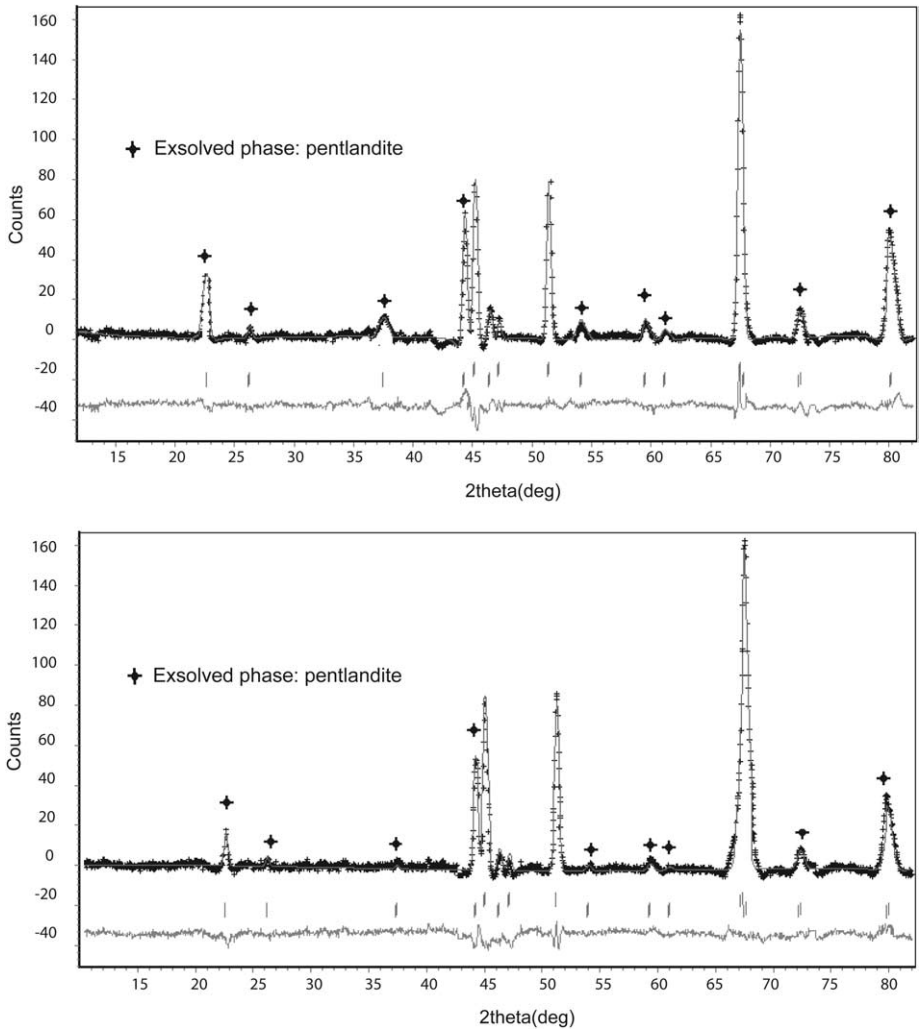

Fig. 1. X-ray diffraction profiles for $(Fe_{0.77}Ni_{0.19})S$ annealed at 473 K (top) and 573 K (bottom) for 500 h. Rietveld refinement of the phase portions gave pentlandite fractions of 33 wt% and 27wt% for 473 and 573 K respectively. Solid curves are the calculated pattern; the experimental data points are +. The difference between the experimental and calculated profiles is shown below. The goodness of fit (GOF) for the two profiles are 0.305 (473 K) and 0.147 (573 K).

quenched to room temperature in cold water. The charges were removed from the tubes and ground to fine powder under acetone ensuring the homogeneity of the *mss*. The samples were then resealed in new silica tubes and heated at 1373 K for 2 h, cooled to 1173 K, annealed for 7 d and then quenched in a large volume of cold water. This resulted in homogenous samples with a relatively uniform grain size of ~0.5 mm. A series of anneal/quench experiments were performed on the *mss* at temperature range from 473 to 573 K with annealing periods up to 500 h. Temperature in the muffle furnaces was controlled within error range ±5 K.

2.2. X-ray Diffraction

Room temperature X-ray powder diffraction patterns of the quenched products were obtained using a 100 mm diameter Guinier Hägg camera with Cr $K_{\alpha 1}$ radiation (λ = 2.2897Å). The finely powdered sample was mixed with a small amount pure Si which was used as an internal standard. The Guinier Hägg films were scanned in TPU/Pos mode using an Epson film scanner and the powder diffraction profiles over 2θ range 10 to 90° were extracted using the programs Scion Image and Universal-Si-Calibration, a macro function based on Igor Pro 4.0 (WaveMetrics Inc.). Weight fraction of exsolved pentlandite was determined by Rietveld refinement (Hunter, 1997). Since all the atoms in the pentlandite structure and *mss*/pyrrhotite subcell occupy special position and Fe and Ni are not readily distinguishable by X-ray diffraction, only profile parameters, cell parameters, overall temperature factor and phase scale factors were refined. The proportions of pentlandite and *mss*/pyrrhotite determined by Rietveld analyses of the X-ray powder diffraction data were compared with the phase analyses obtained on some of the same samples by powder neutron diffraction (Wang et al., 2003) and found to be within one standard deviation. Figure 1 shows the X-ray diffraction patterns for the samples annealed for 500 h at 473 K and 573 K. Note that the pentlandite reflections are more prominent at 473 K than at 573 K.

2.3. Chemical Analyses

Chemical analysis was carried out using a Cameca CAMEBAX SX51 electron microprobe at Adelaide Microscopy, University of Adelaide. The analyses were undertaken using an accelerating potential of 20 kV and a specimen current of ~20 nA. The spot size was set at 1 μm but the effective resolution of the beam, due to beam spread in the sample, was of the order of 3 μm. A natural pentlandite was used as a standard for wavelength dispersive analysis.

Table 1. Exsolution of pentlandite from *mss* $(Fe_{0.77}Ni_{0.19})S$. Summary of results from anneal quench specimens. Pentlandite in weight percentage; a_{penn} a_{pyrr} *and* c_{pyrr} are cell parameters of pentlandite and pyrrhotite. Estimated standard deviations are given in brackets.

Temp (K)	Time (hr)	*wt*% pent.	a_{pent}/Å	a_{pyrr}/Å	c_{pyrr}/Å
473	0.5	0(1)	10.057(3)	3.4461(8)	5.737(3)
	0.75	0(1)	10.059(3)	3.4476(8)	5.736(3)
	1	2(2)	10.060(3)	3.4480(8)	5.733(3)
	2	4(1)	10.064(3)	3.4520(8)	5.730(3)
	5	10(2)	10.058(4)	3.4511(8)	5.722(2)
	26	27(2)	10.063(2)	3.4522(4)	5.725(4)
	46	32(1)	10.070(2)	3.4523(4)	5.720(3)
	64	33(1)	10.067(2)	3.4525(6)	5.719(2)
	100	33(1)	10.070(2)	3.4518(6)	5.721(2)
	500	33(1)	10.068(3)	3.4522(8)	5.720(4)
498	0.5	5(2)	10.062(3)	3.4466(8)	5.725(2)
	1	10(2)	10.060(2)	3.4452(8)	5.726(1)
	8.5	14(3)	10.061(2)	3.4565(8)	5.722(2)
	12	18(2)	10.058(4)	3.4451(8)	5.722(2)
	17	21(2)	10.065(3)	3.5012(8)	5.721(2)
	22.5	25(2)	10.063(2)	3.5112(8)	5.719(2)
	26	25(2)	10.072(1)	3.4449(8)	5.718(2)
	30	27(2)	10.060(3)	3.4450(8)	5.717(3)
	46	30(2)	10.068(4)	3.4453(6)	5.716(2)
	64	29(1)	10.077(2)	3.4455(6)	5.715(2)
	84	31(1)	10.059(2)	3.4457(6)	5.713(1)
	100	31(1)	10.069(2)	3.4448(6)	5.713(1)
523	0.5	6(2)	10.077(1)	3.4464(4)	5.725(3)
	1	17(2)	10.072(4)	3.4501(4)	5.723(1)
	5	21(2)	10.065(2)	3.4502(7)	5.722(2)
	8.5	20(2)	10.072(3)	3.4504(6)	5.722(2)
	12	20(2)	10.069(1)	3.4510(5)	5.721(2)
	17	22(2)	10.067(3)	3.4521(4)	5.719(3)
	22.5	26(2)	10.070(2)	3.4531(5)	5.718(2)
	26	26(2)	10.055(2)	3.4509(7)	5.717(4)
	30	27(2)	10.067(2)	3.4509(6)	5.715(2)
	46	29(1)	10.064(2)	3.4488(6)	5.713(2)
	64	31(2)	10.068(2)	3.4547(8)	5.711(2)
	84	30(1)	10.071(2)	3.4498(3)	5.707(2)
	100	29(1)	10.073(2)	3.4765(6)	5.710(2)
548	0.5	5(2)	10.058(2)	3.4465(4)	5.718(4)
	1	20(2)	10.065(2)	3.4532(2)	5.714(2)
	8.5	22(2)	10.074(4)	3.4501(2)	5.713(2)
	12	24(2)	10.072(3)	3.4520(4)	5.713(2)
	17	26(1)	10.075(2)	3.4502(2)	5.711(2)
	22.5	27(1)	10.073(2)	3.4505(2)	5.711(2)
	26	28(1)	10.074(2)	3.4499(2)	5.710(2)
	30	26(2)	10.077(3)	3.4497(3)	5.708(2)
	46	27(2)	10.068(1)	3.4469(2)	5.707(2)
	64	28(1)	10.071(1)	3.4465(2)	5.708(1)
	100	28(1)	10.071(1)	3.4471(2)	5.708(2)
573	0.5	6(2)	10.061(2)	3.4496(4)	5.719(4)
	1	20(2)	10.063(2)	3.4488(2)	5.717(2)
	2	25(2)	10.068(3)	3.4493(3)	5.717(2)
	5	26(2)	10.071(1)	3.4502(2)	5.716(2)
	26	27(2)	10.073(2)	3.4495(2)	5.712(3)
	46	27(1)	10.074(2)	3.4477(2)	5.708(2)
	64	26(1)	10.073(2)	3.4502(4)	5.708(2)
	100	27(1)	10.065(2)	3.4501(2)	5.707(1)
	500	27(2)	10.070(2)	3.4501(4)	5.707(3)

3. RESULTS AND DISCUSSION

3.1. The Kinetic Model

The cell and phase data for the 5 sets of isothermal annealing experiments are summarized in Table 1. Note that the cell parameters for pentlandite did not change significantly over the course of the reaction indicating that its composition remains more or less constant on the time scale of these experiments. The *c* parameter of pyrrhotite, $c_{pyrr,}$ decreases over the exsolution, as *mss*/pyrrhotite becomes more Fe and vacancy rich. Electron microprobe analysis for the sample annealed at 573 K for 100 h gave the compositions $(Fe_{4.53}Ni_{4.45})S_8$ (S 32.67, Fe 32.30, Ni 33.31 wt%) and $Fe_{0.84}Ni_{0.11}S$ (S 36.84, Fe 53.75, Ni 7.65 wt%) for pentlandite and *mss*/pyrrhotite respectively. This

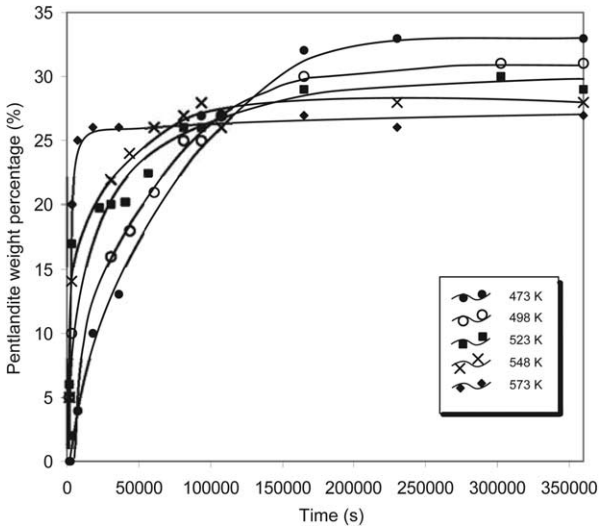

Fig. 2. Graph showing the extent of pentlandite exsolution from *mss*/pyrrhotite (in weight percent) for the five annealing temperatures used: 473 K (●), 498 K (○) 523 K (■), 548 K (×), 573 K (♦). The data were derived by Rietveld refinement of the powder X-ray diffraction profiles. The lines of best fit were calculated by least-square refinement (exponential function in divided sections) using Igor Pro 4.0.

sample had relatively coarse pentlandite lamella and this enabled accurate pentlandite analysis. The electron microprobe analyses also showed that the *mss*/pyrrhotite in this sample was homogeneous; there was no evidence of Fe-Ni compositional gradients between pentlandite lamella. Since the cell parameters of pentlandite do not vary significantly between the five data sets, it can be taken that the pentlandite compositions are the same for all 5 annealing temperatures. The *mss*/pyrrhotite compositions will vary as the final amount of exsolved pentlandite changes with annealing temperature.

Figure 2 shows the amount of pentlandite exsolution plotted against time for 5 temperatures between 473 and 573 K. The exsolution rate in this system is relatively rapid. At the highest temperature, (573 K) the exsolution reaction reaches equilibrium within 5 h (18,000 s), after that period the pentlandite weight fraction remained at around 27%, with little increase even after prolonged annealing. At 473 K the reaction is less rapid and the pentlandite fraction increases continuously to 33 wt% over 24 h.

It is reasonable to believe the same mechanism for exsolution applies over the temperature range, 473 to 573 K, as the samples show very similar textures (Fig. 3).

The weight fraction of pentlandite in Table 1 is converted to reaction extent, *y,* using the equation

$$y = \frac{w_t - w_0}{w_e - w_0} \times 100\% = \frac{w_t}{w_e} \times 100\% (w_0 = 0) \qquad (5)$$

where w_0, w_e, w_t are the weight fractions of pentlandite exsolved at: the beginning of reaction ($t = 0$), at the end of reaction ($t = \infty$) and at an arbitrary time, t, respectively (Yund and Hall, 1970).

A crucial point in kinetic analysis of the data are the definition of w_e. In isothermal exsolutions, the compositions of the host phase *mss*/pyrrhotite will vary with temperature, compositional fields being more extensive with higher temperatures and thus less exsolution will occur. Due to the lack of thermodynamic data for pentlandite-pyrrhotite reactions across the *mss* compositional field, the end of reaction w_e, cannot be determined by *Gibbs* free energy calculations. It is possible to determine w_e by assuming a constant composition of pentlandite and a fixed final composition for *mss*/pyrrhotite, which are independent of temperature and then calculate the mole fractions by mass balance. This approach was employed by Etschmann et al. (2004), who calculated w_e to be 38.78 wt% pentlandite for a pentlandite composition of $(Fe_{4.5},Ni_{4.5})S_8$ and a Ni-free *mss*/pyrrhotite. This mode of a fixed extent of reaction independent of temperature is unrealistic, as at higher temperatures the reactions will never reach completion and this can result in apparently negative activation energies.

The alternative is to define equilibrium for the process empirically from the experiments and make no assumptions about the compositions of the pentlandite and *mss*/pyrrhotite.

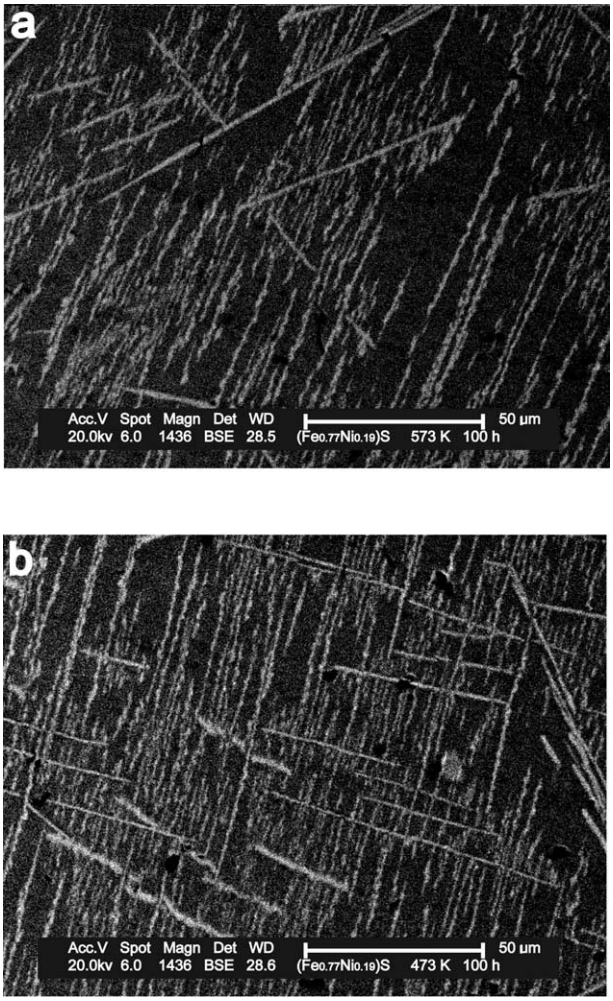

Fig. 3. Back Scattered Electron (BSE) images showing the pentlandite/pyrrhotite exsolution textures for $(Fe_{0.77}Ni_{0.19})S$ annealed at (a) 573 K and (b) 473 K for 100 h. Pentlandite lamella (light) in *mss*/pyrrhotite host (dark). The similarity of the textures at both temperatures indicates that similar exsolution mechanism applies over the temperature range 473 to 573 K.

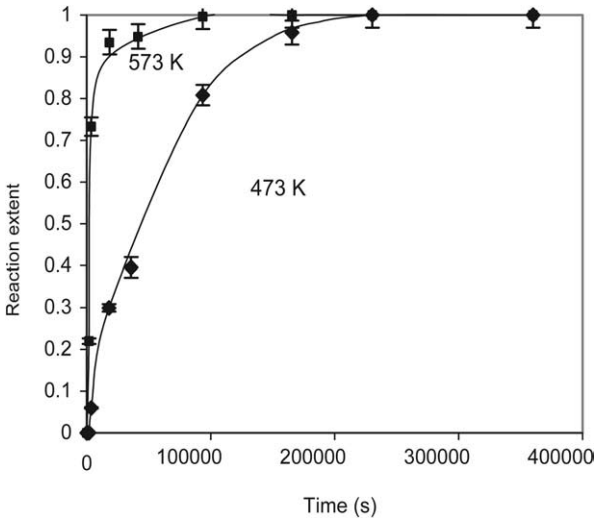

Fig. 4. Plot of reaction extent of pentlandite exsolution (y) against time (t) for annealing experiments at 473 and 573 K. The curves are derived from the data in Table 1 and Figure 2. The pentlandite weight fractions are converted to reaction extent using Eqn. 5. Data measured at 473 and 573 K are represented by symbols ♦ and ■ with error bar.

The classic Avrami model describes the exponential relationship between y (reaction extent) and t (time), but this relation is, theoretically, not valid for infinitively long reaction times (Yund and Hall, 1970). For heterogeneous solid reactions, w_e should be selected at the phase fractions when the portion of pentlandite exsolution has leveled out. The phase fractions from the annealing experiments at 473 and 573 K change very little after 24 h. In these experiments w_e was defined as the average amount of pentlandite exsolved during the three longest annealing periods at each temperature (Table 1). Converting pentlandite weight fraction to reaction extent, y, vs. time, using the above method gives the plots in Figure 4.

3.2. Kinetic Analysis Using the Refined Avrami Method

Many traditional kinetic models assume the overall activation energy of solid-state reaction does not vary during the course of reaction. This assumption ignores the fact that activation energy depends on the structural environment around the atoms, and that this may change significantly during the reaction. Vyazovkin and Lesnikovich (1990) showed that revealing the dependence of the activation energy (E_a) on reaction extent (y), helps not only to understand the complexity of a reaction process, but also identify its kinetics scheme. During the course of exsolution, Ni and Fe atoms diffuse out of the *mss*/pyrrhotite into pentlandite and the *mss*/pyrrhotite becomes progressively more metal deficient and richer in Fe as the reaction proceeds. The local chemical environment of Ni and Fe atoms in *mss*/pyrrhotite changes in the second coordination sphere as the Ni fraction falls from 0.20 to 0.11 during exsolution. More importantly, the concentration of metal vacancies in *mss*/pyrrhotite increases from 3 to 5% of cation sites and thus, E_a for metal diffusion would be expected to decrease. This should lead to a decrease in the overall activation energy as y increases.

On the premise that E_a is a function of reaction extent, y, we can adjust the Arrhenius equation as follows:

$$k(T, y) = A\exp\left[-\frac{E_a(y)}{RT}\right] \tag{6}$$

Assuming the plot against t in Figure 5 conforms to the classic Avrami equation, we can rewrite the Avrami Eqn. 1 as

$$\ln\ln\left(1/(1-y)\right) = n\ln k + n\ln t \tag{7}$$

If Eqn. 7 applies, then a plot of lnln[1/(1 − yr)] vs. ln$t$ should be linear. Clearly, from the plot in Figure 5, it is not, even when experimental uncertainties are considered. Also, the reaction curves in Figure 2 do not comply with the classic Avrami model. The experimental curves show simply decelerating reaction rates during the reactions while the classic Avrami model (Eqn. 1) has a sigmoidal form (n ≠ 1). Reaction curves described by the classic Avrami Eqn. 1 undergo a distinct induction period with a low reaction rate at the beginning, then accelerate to a maximum, and finally approach zero as the reaction reaches completion.

Therefore, we need to consider a modification of the classic Avrami method.

The basic kinetic equation is

$$\frac{dy}{dt} = k(T, y)\cdot f(y) \tag{8}$$

T is temperature; $k(T,y)$, rate constant; $f(y)$, a kinetic model. Rewriting Eqn. 8 and substituting Eqn. 6 for $k(T,y)$ gives,

$$\ln\frac{dy}{dt} = \ln A + \ln f(y) - \frac{E_a(y)}{RT} \tag{9}$$

For a given reaction extent $y = y_0$, ln $f(y)$ and $E_a(y_O)$ are constant. Therefore,

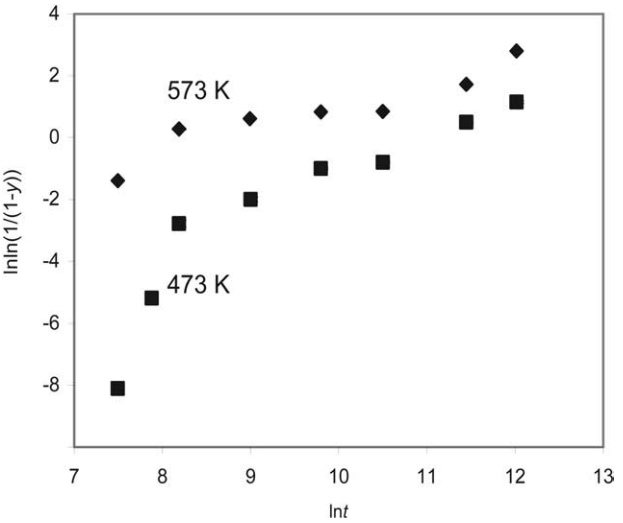

Fig. 5. The plot of lnln[1/(1 − y)] against ln$t$ for the pentlandite exsolution at 473 and 573 K. Reaction extent (y), time (t). It appears that the variation of lnln[1/(1 − y)] with ln$t$ does not follow a linear relation as the classic Avrami method requires.

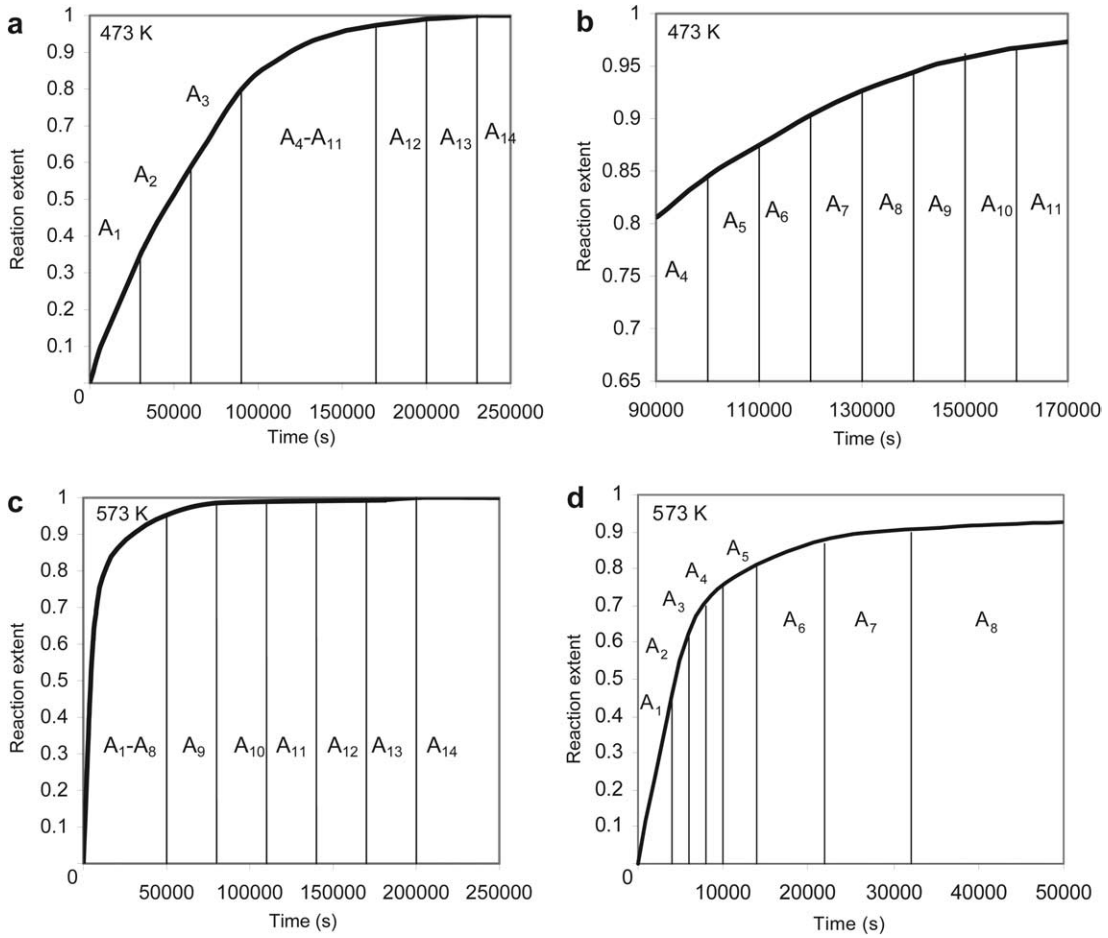

Fig. 6. The curves describing the exsolution of pentlandite at 473 and 573 K (Fig. 4) are subdivided into small regions where the slope is approximately constant. Regions $A_4 \sim A_{11}$ at 473 K and A_1-A_8 at 573 K are finely subdivided due to the relative sharpness of these parts of the curves. (a) exsolution lines at 473 K. (b) enlargement of region A_4-A_{11} in (a). (c) exsolution lines at 573 K. (d) Enlargement of region A_1-A_8 in (c). The curves are derived by least-square method (exponential function in divided sections) using Igor Pro 4.0 to fit exsolution data at 473 and 573 K in Table 1.

$$E_a(y_0) = -R\frac{\ln \dfrac{dy}{dt}(y_0, T_1) - \ln \dfrac{dy}{dt}(y_0, T_2)}{\left(\dfrac{1}{T_1} - \dfrac{1}{T_2}\right)} \qquad (10)$$

where $dy/dt(y_0, T_1)$ and $dy/dt(y_o, T_2)$ are reaction rates to a given value of y_0 at two different temperatures (473 and 573 K respectively). Assuming that the reaction mechanism does not change significantly over the temperature range, the plots in Figure 4 functionally relate the reaction extent y and the annealing time, t, at 473 K and 573 K. The time to a given reaction extent y_0 can therefore be extrapolated from these plots.

Applying Eqn. 10 to calculate activation energy relies on the determination of dy/dt. With careful inspection of the exsolution graph in Figure 4 we find that $\tilde{y}y(t)$ can be divided into a series of regions. This is achieved by dividing the raw data into small time segments, such that the $y = y(t)$ curve can be approximated as a straight line and the slope of each segment is the reaction rate dy/dt. Each region has a nearly constant slope (dy/dt) and this is shown in Figure 6. The calculated reaction rates are plotted against y for the reactions at 473 K and 573 K and are shown in Figure 7. The reaction rates vary from 1.6×10^{-5} to 5.0×10^{-7} s^{-1} at 473 K and 9.4×10^{-5} to 4.1×10^{-7} s^{-1} at 573 K. These reaction rates are slower than those reported by Etschmann et at. (2004) for pentlandite exsolution with M:S of 1:1. The activation energies, determined using Eqn. 10 are summarized in Table 2 and the dependence on y are plotted in Figure 8.

At the beginning of reaction, E_a is around 49.4 kJ.mol^{-1}, but decreases gradually to around 20.7 kJ.mol^{-1} as y approaches 1.

This situation is different from that found by Etschmann et al. (2004) where the bulk composition of their *mss*/pyrrhotite was $(Fe_{0.8}Ni_{0.2})S$, equal amounts of metal and sulfur and thus very few metal vacancies. Heating this material creates S vacancies, and thus local sites of metal enrichment for nucleation of pentlandite, a metal rich mineral. This more metal rich system, $Fe_{0.8}Ni_{0.2}S$ shows a variation of E_a from 2.0 to 21.0 kJ.mol^{-1} (Fig. 9). The low value of E_a (2.0 kJ.mol^{-1}) at the beginning of reaction is consistent with a much lower

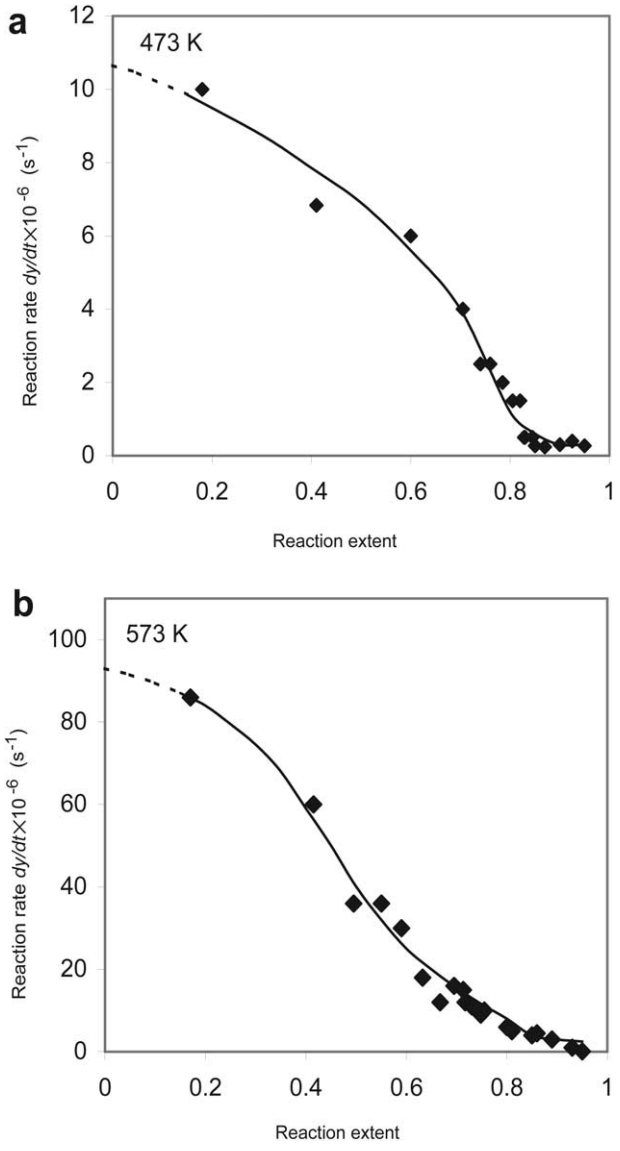

Fig. 7. Plot of reaction rate against reaction extent (y) at 473 and 573 K. Reaction rate (dy/dt) is calculated from the slope of $\bar{y}t$ at each time region $A_1 \sim A_{14}$ in Figure 6. The solid curves are produced by least-square method (Hill function) using Igor Pro 4.0 to fit the calculated dy/dt values in time segments $A_1 \sim A_{14}$.

nucleation energy barrier and consistent with a nucleation model based on S vacancies forming local sites of metal enrichment. The activation energy gradually approaches to an asymptotic value 21.0 kJ.mol^{-1} at the end of reaction. This value is comparable with the value of E_a (20.7 kJ.mol^{-1}) in our current study as the reaction approaches completion. In the metal poor composition investigated here, heating of the sample also will create S vacancies, but these are compensated by the existing metal vacancies and the local areas of metal enrichment that trigger pentlandite nucleation are much more difficult to form.

For $(Fe_{0.77}Ni_{0.19})S$, it appears that E_a is relatively constant at the beginning of exsolution as nucleation of pentlandite is the decisive step. Once $y > 0.5$ it is reasonable to assume that

Table 2. Annealing time and overall activation energy at various fractions of the reaction at T_1 = 473 and T_2, 573 K.

y_o/%	$t(y_o, T_1)$/s	$t(y_o, T_2)$/s	E_a (y_o)/kJ · mol^{-1}
0	0	0	—
0.10	6588	980	48.86
0.15	13482	1471	49.12
0.20	15333	1960	49.32
0.25	19321	2451	49.47
0.30	23130	2941	49.61
0.35	30120	3436	49.35
0.40	35010	3827	48.34
0.45	43221	4101	48.44
0.50	48569	4832	46.48
0.55	56370	5392	44.33
0.60	63124	5882	41.95
0.65	69547	6842	37.74
0.70	78828	8102	32.81
0.75	84466	9580	28.43
0.80	90123	12890	23.67
0.85	100123	19522	21.54
0.90	119985	31000	21.03
0.95	146912	69124	20.66

lamellae coarsening is dominant. As the reaction proceeds, the concentration of metal vacancies in *mss*/pyrrhotite increases and the diffusion path for the metal ions becomes easier. The observation that the reaction rate (dy/dt) slows towards the end of reaction does not conflict with the conclusion of decreasing E_a. The decreasing reaction rate as the reaction approaches equilibrium or at metastable equilibrium is linked to the extended compositional field of *mss* at these annealing temperatures. Both our experiments and those of Etschmann et al. (2004) converge to common residual *mss* compositions and a common value of E_a. The decreasing reaction rate does not appear to be due to increasing path length for Ni and Fe diffusion in mss/pyrrhotite. Under such circumstances, it would be reasonable to expect Ni or Fe composition gradients in

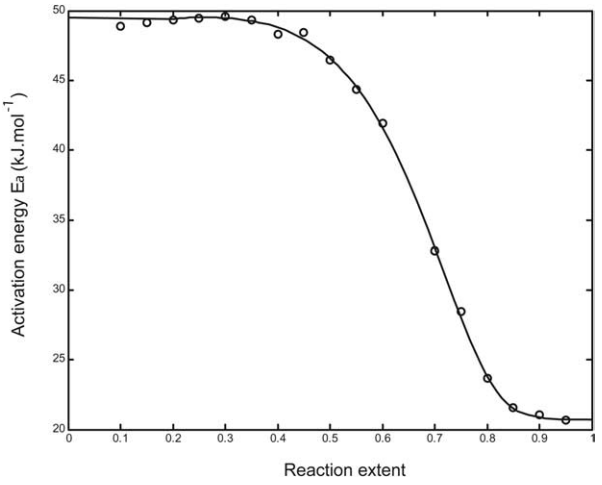

Fig. 8. Graph showing the dependence of E_a (activation energy) on y for the pentlandite exsolution from *mss*/pyrrhotite (initial bulk composition $(Fe_{0.77}Ni_{0.19})S$). The calculated values of activation energy using the refined Avrami method are represented by symbol ○. The solid curves are produced by least-square method (sigmoid function) using Igor Pro 4.0 to fit the calculated value of E_a.

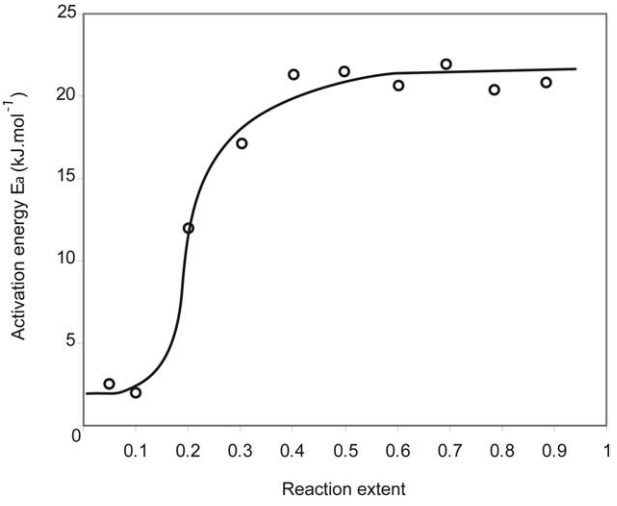

Fig. 9. Graph showing dependence of E_a (activation energy) on y for the pentlandite exsolution from *mss*/pyrrhotite (initial bulk composition $(Fe_{0.8}Ni_{0.2})S$). Raw data are from Etschmann et al. (2004). The calculated values of activation energy using the refined Avrami method are represented by symbol ○. The solid curves are produced by least-square method (sigmoid function) using Igor Pro 4.0 to fit the calculated value of E_a.

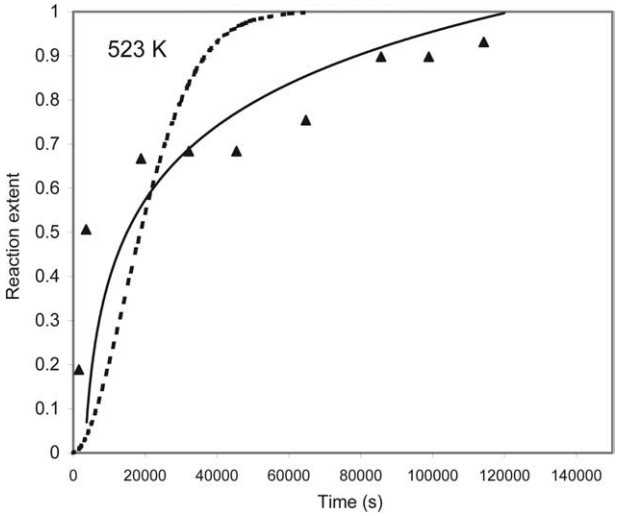

Fig. 10. Predicted kinetic curves for the exsolution of pentlandite from *mss*/pyrrhotite at 523 K. Continuous line is the prediction using the refined Avrami method and the dash line is the prediction using the classic Avrami method, and triangles are experimental data.

mss/pyrrhotite samples annealed for long periods. A series of line scans during electron microprobe analyses failed to find any evidence of such gradients, the composition of *mss*/pyrrhotite was homogenous.

The dependence of E_a on y can be used to predict kinetic behavior at any arbitrary intermediate temperature assuming the reaction mechanism has not changed.

We denote this method, the refined Avrami method, and it employs the concept that E_a changes with reaction extent y. The original Avrami Eqn. 1 can be rewritten as,

$$t(y_0, T) = \exp\left[\frac{E_a(y_0)}{R}\left(\frac{1}{T} - \frac{1}{T_1}\right) + \ln\, t(y_0, T_1)\right] \quad (11)$$

If, $T_1 = 473$ K then

$$t(y_0, T) = \exp\left[\frac{E_a(y_0)}{R}\left(\frac{1}{T} - 0.002113\right) + \ln\, t(y_0, 473\ \text{K})\right] \quad (12)$$

Calculated from Eqn. 12 with data $E_a = E_a(y)$ in Table 2, the predicted variation of y with t at $T = 498$, 523 and 548 K are given in Table 3.

The difference between the kinetic behavior predicted using the classic Avrami method and the refined Avrami method is shown in Figure 10, where the predicted curves of both methods are compared with experimental data obtained at 523 K. Clearly, the refined Avrami method produces a better fit to the

Table 3. Predicted kinetic data for the exsolution of pentlandite fro m *mss* $(Fe_{0.77}Ni_{0.19})S$ at temperatures 498, 523, and 548 K.

y_o/%	$E_a(y_o)$/kJ · mol^{-1}	$t(y_0, 498\ \text{K})$/s	$t(y_o, 523\ \text{K})$/s	$t(y_o, 548\ \text{K})$/s
0	—	0	0	0
0.10	48.86	3532	2010	1204
0.15	49.12	7204	4087	2442
0.20	49.32	8172	4626	2758
0.25	49.47	10278	5808	3457
0.30	49.61	12283	6929	4119
0.35	49.35	16048	9081	5412
0.40	48.34	18895	10817	6516
0.45	48.44	23297	13322	8016
0.50	46.48	26843	15700	9644
0.55	44.33	32021	19199	12062
0.60	41.95	36963	22780	14673
0.65	37.74	42971	27801	18715
0.70	32.81	51867	35521	25181
0.75	28.43	58771	42335	31422
0.80	23.67	66633	50708	39563
0.85	21.54	76066	59327	47332
0.90	21.03	91751	71982	57737
0.95	20.66	112873	88933	71610

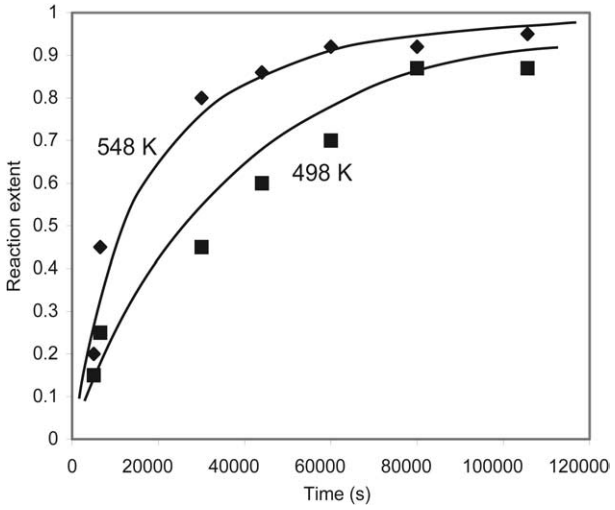

Fig. 11. Plot showing the predicted kinetics exsolution of pentlandite from *mss*/pyrrhotite exsolution at 498 and 548 K using the refined Avrami method together with the experimental values. The solid lines are the theoretical predictions using the refined Avrami method. Squares and diamonds are experimental results at 498 and 548 K, respectively.

isothermal data than the classic Avrami method. Isothermal data were also collected at two other temperatures, 498 and 548 K, and these are illustrated in Figure 11. Again the correspondence between experimental data and prediction is excellent using the refined Avrami method.

Overall, the exsolution process is a multi-step reaction dependent on many other factors in addition to nucleation and metal diffusion. These experiments, however, do illustrate that the widely used assumption of constant activation energy during reaction is very approximate. It is worth emphasizing that most mineral reactions are heterogenous, involving the nucleation and growth of new phases, separated by new surfaces or interfaces. Such reactions involve at least two or often more consecutive steps, each with its own activation energy. In sequential reactions the overall reaction rate is determined by the slowest step and hence an experimentally determined activation energy or rate constant would most probably refer to this 'rate-determining' step (Yund and McCallister, 1970). In the pentlandite-pyrrhotite system, the nucleation and ion diffusion are more than just sequential steps. At the beginning of reaction, pentlandite nucleation is followed by crystal growth (driven by Fe/Ni diffusion) and as the reaction proceeds nucleation becomes less important and crystal growth will dominate. In most cases, the overall activation energy is some intermediate value if more than one step is compatible with the slowest step. Therefore, the contributions of each step to the reaction mechanism are nearly impossible to determine. To gain an understanding of these solid-state reactions it is important to extract the activation energy independent of any reaction model.

Apart from isothermal methods, nonisothermal experiments are also widely used to study reaction kinetics. Vyazovkin (1997) shows how isoconversional methods can be used to predict the kinetic behavior of a reaction outside of the range of experimental temperatures. Model free methods can be adopted to avoid any arbitrary decision in choosing an over simplified model.

3.3. The Effects of S Fugacity on the Kinetics of Exsolution

The experimental results for the exsolution of pentlandite from a *mss*/pyrrhotite, of composition $(Fe_{0.77}Ni_{0.19})S$, show reaction rates vary from 1.6×10^{-5} to 5.0×10^{-7} s^{-1} at 473 K and from 9.4×10^{-5} to 4.1×10^{-7} s^{-1} at 573 K. These rate constants can be compared with those of Etschmann et al. (2004) who found rates of 8×10^{-6} s^{-1} for exsolution from a *mss* of a more metal rich composition $(Fe_{0.8}Ni_{0.2})S$. Etschmann et al. (2004) also recalculated the data from a set of isothermal experiments at 673 K on *mss* compositions $(Fe_{0.89}Ni_{0.11})_{1-x}S$ reported by Kelly and Vaughan (1983). They examined 4 different M:S ratios, with x in the range $0.0 \leq x \leq 0.05$ and the rate constants calculated from their data vary from 3×10^{-5} to 1×10^{-6} s^{-1} between $0.0 \leq x \leq 0.035$, with the slowest rate for the most S rich composition, $x = 0.035$. For $x = 0.05$ no exsolution was observed on the time scale of their annealing runs (1000 h). Our results, taken with those of Etschmann et al. (2004) and Kelly and Vaughan (1983), show that an increase in S fugacity (f_s) decreases the rate of exsolution. Etschmann et al. (2004) concluded that the decrease in rate with increasing f_s is associated with a change in the nucleation mechanism. For *mss*/pyrrhotite with M:S ratios near to 1:1, heating to 573 K creates S vacancies in the *mss* $(Fe,Ni)S_{1-x}$, even in a closed evacuated system. This triggers nucleation of pentlandite, a metal rich mineral and facilitates nucleation. Examination of the exsolution textures confirms different nucleation mechanisms for different sulfur to metal ratios (see Durazzo and Taylor, 1982; Etschmann et al., 2004). On the other hand, increasing S content results in a greater concentration of cation vacancies that will facilitate metal diffusion. Etschmann et al. (2004), using the classic Avrami method, calculated an approximate E_a for the exsolution of 5.0 $kJ.mol^{-1}$. However using the refined Avrami method, E_a varies from 2.0 to 21.0 $kJ.mol^{-1}$. The increase in E_a with y is related to the nucleation dominant stage at the beginning of reaction, and crystal growth controlled stage at the end. The in situ cooling and high temperature annealing experiments of Etschmann et al. (2004) showed that, after the initial exsolution, some of the pentlandite is resorbed indicating a high degree of supersaturation in the solid solution with M:S ratio of 1:1. The differences in E_a for pentlandite exsolution from $(Fe_{0.8}Ni_{0.2})S$ and $(Fe_{0.77}Ni_{0.19})S$ reflect the change of nucleation mechanism, from S vacancies to grain boundaries and S vacancies with the richer S compositions.

Overall our data and the work by Etschmann et al. (2004), and Yund and Hall (1970) indicate that low exsolution activation energies prevail in the pyrrhotite/pentlandite/pyrite system, although further experimental data are required to draw such general conclusions.

4. CONCLUSION

The pentlandite-*mss*/pyrrhotite exsolution reaction has multiple steps: nucleation, new phase growth and atomic diffusion, lamellae coarsening. These make its kinetic analysis difficult, as the mechanisms cannot be elucidated in detail. In mineral

reactions of this type the true functional form of the reaction model is almost never known, and the Arrhenius parameters determined by the classic Avrami method are skewed to compensate for errors in the model. The refined Avrami method employs the important concept that activation energy depends on reaction extent y. Kinetic study of pentlandite exsolution from *mss*/pyrrhotite was performed for the low temperature range from 473 to 573 K. For *mss*/pyrrhotite with bulk composition $(Fe_{0.77}Ni_{0.19})S$, activation energy of pentlandite exsolution, E_a varies from 49.6 kJ.mol^{-1} at the beginning of reaction (nucleation is dominant) to 20.7 kJ.mol^{-1} at the end (crystal growth is dominant).

In general, the activation energy varies during the course of solid reaction with the extent of reaction. The surrounding environment of reactant atoms affects the atom's activity and more or less account for changes of activation energy E_a. We are currently applying this refined Avrami method to further study of the pentlandite-*mss*/pyrrhotite and pyrite-pyrrhotite systems, where constancy of E_a fails to reveal details of the exsolution kinetics.

Acknowledgments—The authors wish to thank Barbara Etschmann and Andrew Putnis for the assistance with data collection and valued advice. We thank Prof. D.J. Vaughan and the three anonymous referees for their valuable comments and suggestions. This work is financially supported by Australian Research Council and Australian Institute for Nuclear Science and Engineering.

Associate editor: David Vaughan

REFERENCES

Arnold R. G. (1962) Equilibrium relations between pyrrhotite and pyrite from 325 to 743°C. *Econ. Geol.* **75,** 72–90.

Avrami M. (1939) Kinetics of phase change I. *J. Chem. Phys.* **7,** 1103–1112.

Avrami M. (1940) Kinetics of phase change II. *J. Chem. Phys.* **8,** 212–224.

Avrami M. (1941) Granulation, phase change and microstructure. *J. Chem. Phys.* **9,** 177–184.

Burke J. (1965) *The Kinetics of Phase Transformations in Metals*. Pergamon Press.

Christian J. W. (1965) *The Theory of Transformations in Metals and Alloys*. Pergamon Press.

Craig J. R. (1973) Pyrite-pentlandite assemblages and other low temperature relations in the Fe-Ni-S system. *Am. J. Sci.* **273A,** 496–510.

Doyle C. D. (1961) Kinetic analysis of thermogravimetric data. *J. Appl. Polym. Sci.* **5,** 285–292.

Durazzo A. and Taylor L. A. (1982) Exsolution in the *mss*/pyrrhotite-pentlandite system: Textural and genetic implications for Ni-sulfide ores. *Min. Dep.* **17,** 313–332.

Etschmann B., Pring A., Putnis A., Grguric B. A., and Studer A. (2004) A kinetic study of the exsolution of pentlandite $(Ni,Fe)_9S_8$ from the monosulfide solid solution (Fe,Ni)S. *Am. Mineral.* **89,** 39–50.

Farrell S. P. and Fleet M. E. (2002) Phase separation in $(Fe, Co)_{1-x}$ monosulfide solid-solution below 450°C, with consequences for coexisting pyrrhotite and pentlandite in magmatic sulfide deposits. *Can. Mineral.* **40,** 33–46.

Fleet M. S. (1968) On the lattice parameters and superstructures of pyrrhotites. *Am. Mineral.* **53,** 1846–1855.

Francis C. A., Fleet M. E., Misra K., and Craig J. R. (1976) Orientation of exsolved pentlandite in natural and synthetic nickeliferous pyrrhotite. *Am. Mineral.* **61,** 913–920.

Friedman H. (1964) Kinetics of thermal degradation of char-forming plastics from thermogravimetry: Application to a phenolic plastic. *J. Polym. Sci. C.* **6,** 183–195.

Hunter B. A. (1997) Rietica for Windows, ANSTO Press, Sydney. pp. 1–22.

Kelly D. P. and Vaughan D. J. (1983) Pyrrhotine-pentlandite ore textures: A mechanistic approach. *Min. Mag.* **47,** 453–463.

Kullerud G. (1971) Experimental techniques in dry sulfide research. In *Research Techniques for High Pressure and High Temperature* pp. 288–315 (ed. G. C. Ulmer). Springer-Verlag.

Misra K. C. and Fleet M. E. (1973a) The chemical composition of synthetic and natural pentlandite assemblages. *Econ. Geol.* **68,** 518–539.

Misra K. C. and Fleet M. E. (1973b) Unit cell parameters of monosulfide, pentlandite and taenaite solid solutions within the Fe-Ni-S system. *Mater. Res. Bull.* **8,** 669–678.

Naldrett A. C., Craig J. R., and Kullerud G. (1967) The central portion of the Fe-Ni-S system and its bearing on pentlandite exsolution in iron-nickel sulfide ores. *Econ. Geol.* **62,** 826–847.

Ozawa T. (1965) A new method of analyzing thermogravimetric data. *Bull. Chem. Soc. Jpn.* **38,** 1881–1886.

Putnis A. (1992) *Introduction to Mineral Science.* Cambridge University Press.

Rajamani V. and Prewitt C. T. (1973) Crystal chemistry of natural pentlandites. *Can. Mineral.* **12,** 178–187.

Riley J. F. (1977) The pentlandite group $(Fe,Ni,Co)_9S_8$: New data and an appraisal of structure-composition relationships. *Min. Mag.* **41,** 345–349.

Toulmin P. □. and Barton P. B. (1964) A thermodynamic study of pyrite and pyrrhotite. *Geochim. Cosmochim. Acta* **28,** 641–671.

Vaughan D. J. and Craig J. R. (1974) The crystal chemistry and magnetic properties of iron in the monosulfide solid solution of the Fe-Ni-S system. *Am. Mineral.* **59,** 926–933.

Vaughan D. J. and Craig J. R. (1978) *Mineral Chemistry of Metal Sulfides*. Cambridge University Press.

Vyazovkin S. (1997) Evaluation of activation energy of thermally stimulated solid-state reactions under arbitrary variation of temperature. *J. Comput. Chem.* **18,** 393–402.

Vyazovkin S. (2000a) On the phenomenon of variable activation energy for condensed phase reactions. *New J. Chem.* **24,** 913–917.

Vyazovkin S. (2000b) Kinetic concepts of thermally stimulated reactions in solids: A view from a historical perspective. *Int. Rev. Phys. Chem.* **19,** 45–60.

Vyazovkin S. (2001) Modification of the integral isoconversional method to account for variation in the activation energy. *J. Comput. Chem.* **22,** 178–183.

Vyazovkin S. (2003) Reply to "what is meant by the term 'variable activation energy' when applied in the kinetics analyses of solid state decompositions (crystolysis reactions)?" *Thermochim. Acta* **392,** 269–271.

Vyazovkin S. and Lesnikovich A. (1990) Error in determining activation energy caused by the wrong choice of process model. *Thermochim. Acta* **165,** 273–80.

Vyazovkin S. and Dollimore D. (1996) Linear and nonlinear procedures in isoconversional computations of the activation energy of nonisothermal reactions in solids. *J. Chem. Inf. Comput. Sci.* **36,** 42–45.

Vyazovkin S. and Wright C. A. (1997) Kinetics in solids. *Annu. Rev. Phys. Chem.* **48,** 125–149.

Wang H., Ngothai Y., O'Neill B. and Pring A. (2003) The effects of S fugacity on the exsolution of pentlandite $(Fe, Ni)_9S_8$ from the monosulfide solid solution(Fe,Ni)S. Presented at CHEMECA 2003, 31st Annual Australian Chemical Engineering Conference, Adelaide, Australia.

Wiersma C. L. and Rimstidt J. D. (1984) Rates of reaction of pyrite and marcasite with ferric iron at pH 2. *Geochim. Cosmochim. Acta* **48,** 85–92.

Yund R. A. and Hall H. T. (1970) Kinetics and mechanism of pyrite exsolution from pyrrhotite. *J. Petrol.* **11,** 381–404.

Yund R. A. and McCallister R. H. (1970) Kinetics and mechanisms of exsolution. *Chem. Geol.* **6,** 5–30.